

# Bond Graphs for multi-physics informed Neural Networks for multi-variate time series

Alexis-Raja Brachet<sup>a,b,\*</sup>, Pierre-Yves Richard<sup>b</sup> and Céline Hudelot<sup>a</sup>

<sup>a</sup>MICS, CentraleSupélec, Université Paris-Saclay, France

<sup>b</sup>CentraleSupélec, IETR UMR CNRS 6164, France

**Abstract.** In the trend of hybrid Artificial Intelligence (AI) techniques, Physic Informed Machine Learning has seen a growing interest. It operates mainly by imposing a data, learning or inductive bias with simulation data, Partial Differential Equations or equivariance and invariance properties. While these models have shown great success on tasks involving one physical domain such as fluid dynamics, existing methods still struggle on tasks with complex multi-physical and multi-domain phenomena. To address this challenge, we propose to leverage Bond Graphs, a multi-physics modeling approach together with Graph Neural Network. We thus propose Neural Bond Graph Encoder (NBgE), a model agnostic physical-informed encoder tailored for multi-physics systems. It provides an unified framework for any multi-physics informed AI with a graph encoder readable for any deep learning model. Our experiments on two challenging multi-domain physical systems - a Direct Current Motor and the Respiratory system - demonstrate the effectiveness of our approach on a multi-variate time series forecasting task.

## 1 Introduction

In recent years, deep neural machine learning has shown great success in processing data in various tasks. In the engineering field, recent attempts on challenging tasks have shown the need to combine deep neural models with human knowledge, an approach named Informed Machine Learning. In our paper, we consider physical knowledge, positioning us in the Physical-Informed Machine Learning (PIML) field [14].

PIML attempts can be divided into three main classes according to the type of inductive bias from knowledge: data bias, learning bias and architecture bias [14]. Data bias mainly consists of generating simulated data. A typical learning bias approach is a Physical-Informed Neural Network (PINN) [23] leveraging Differential Equations in training objectives. Architecture bias incorporates physical properties such as equivariances and invariances to transformations to the neural model. These approaches have shown performances in fluid dynamics [23] or material discovery [16] in particular in the *some data, some knowledge* paradigm [14].

When multi-physical systems are involved, these models are still struggling. However, in the physical modeling field, some formalisms have been proposed to unify physical systems representations among which the Bond Graph formalism [22] built on the shared notion of energetic power. It provides a domain-independent representation of any multi-physical system. For instance, [24] model

\* Corresponding Author. Email: alexisraja.brachet@centralesupelec.fr.

the whole cardiovascular system in a unique bond graph involving fluid mechanics, chemical reactions, electricity, and mechanical deformation. Nevertheless, to our knowledge, hybridation between Bond graphs and deep neural networks is under-studied. This paper is a first attempt to answer this limitation.

Following the current ML community trend, which consists of learning representation, we first propose to work on a physical-informed encoder. We introduce NBgE, a new architecture that combines bond graphs with Message Passing Graph Neural Networks. In addition to being the first - to our knowledge - unified framework that incorporates multi-physics in a unique architecture, it is also a model-agnostic encoder, that can be plugged into any task-specific model. We demonstrate its effectiveness on a multi-variate time series forecasting task on two challenging multi-physics systems: a Direct Current (DC) Motor and the Respiratory system.

We organize this paper as it follows: in Section 2 we recall the main principles of the bond graph formalism and of Graph Neural Networks (GNNs). In Section 3, we develop the NBgE architecture by introducing the Bond Matrix (Section 3.2), then the dual graph generation process (Section 3.3) and the definition of the Bond Graph Convolution (BGC) (Section 3.4), the core of the NBgE (Section 3.5). We then conduct experiments in Section 4 to empirically validate the performances of the NBgE in the case of a DC motor (own dataset) and the human respiratory system (public dataset), two challenging multi-physical systems. The overall pipeline is detailed in Figure 1.

## 2 Theoretical preliminaries

### 2.1 Preliminaries on Bond graphs

A bond graph  $\mathcal{BG}(\mathcal{C}, \mathcal{B})$  is a directed node-edge-attributed graph composed of a set of nodes  $\mathcal{C}$  that represents the different components of the system and a set of bonds  $\mathcal{B} \subseteq \mathcal{C} \times \mathcal{C}$  representing the power exchanges between the components.

Each bond has 4 attributes  $(k(b), e, f, |)$ : id, effort and flow variables, and causal stroke.  $e$  and  $f$  are physical signals. They are continuous and bounded with respect to time, thus, for any signal acquisition if time  $T \in \mathbb{R}_+^*$ ,  $\int_{[0, T]} e(\tau) d\tau < +\infty$  and  $\int_{[0, T]} f(\tau) d\tau < +\infty$ . Power is defined as  $P = e.f$ . The causal stroke sets the direction of effort and flow signals between the two components (nodes) connected by the bond (edge). Given a bond connecting two components  $\mathcal{C}_1$  and  $\mathcal{C}_2$ , if the causal stroke is at  $\mathcal{C}_1$ 's end, then it receives the effort from  $\mathcal{C}_2$  and it gives back the flow and vice versa.

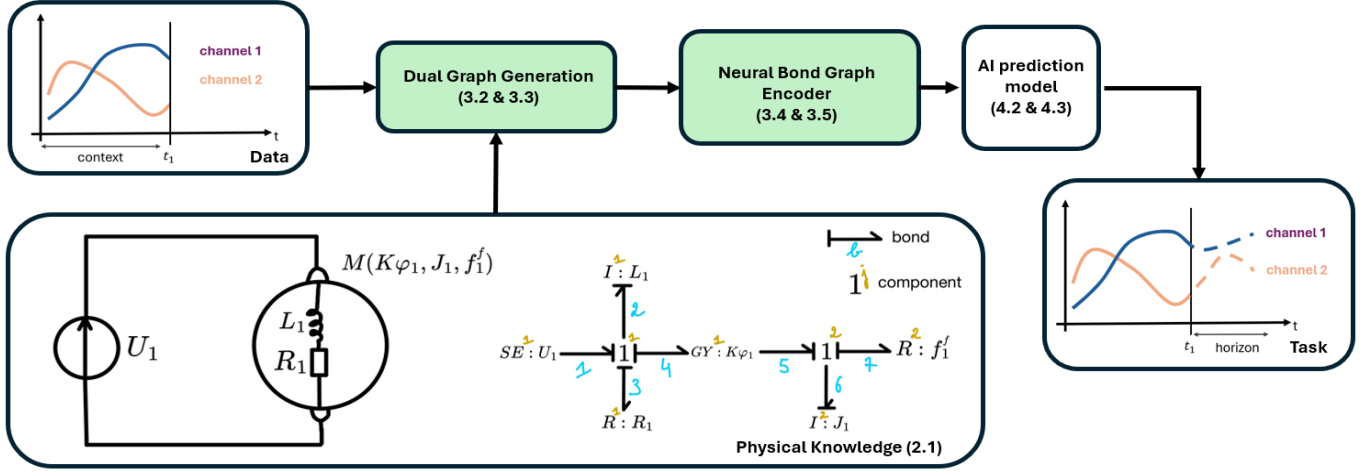


**Figure 1.** The Neural Bond Graph Encoder pipeline. A dual graph is generated from the input data and the Bond Graph of the system, gathering the data and the physical knowledge. Then, NBgE encodes the input data with the Bond Graph Convolution defined on top of the dual graph. The encoded data feeds any AI model for the time series forecasting task.

Each node  $C$  has 3 attributes  $(c(C), k(c(C)), \varphi_C)$ : component type, id (depending on the component type), and the way it processes effort and flow variables of the edges connected to it.

A component  $C \in \mathcal{C}$  can be an element or a junction. There are 5 types of elements depending on the relation they impose between the effort and the flow [8]. **Sources of effort (SE)** and **sources of flow (SF)** are source elements: effort and flow of the bonds attached to a source are independent. **Resistances (R)** are physical elements in which effort and the flow are related by the equation:  $\varphi_R(e, f) = 0$ ; **inertias (I)** are components in which  $\varphi_I(\int_t e(\tau)d\tau, f) = 0$ ; and **capacitances (C)** are components in which  $\varphi_C(\int_t f(\tau)d\tau, e) = 0$ .

Then, there are four main types of junctions, distinguished by how power is distributed among the bonds connected at the same junction [8]. For any bonds  $i$  and  $j$  connected to a **0-junction**,  $\varphi_{0,1}(e_i, e_j) = e_i - e_j = 0$  (unique characteristic effort). Additionally, flow is balanced between the  $n$  bonds connected to it:  $\varphi_{0,2}(f_1, \dots, f_n) = \sum_i a_i f_i = 0$  with  $a_i = 1$  if the bond is directed towards the junction,  $a_i = -1$  otherwise. **1-junctions** follow similar principles but with flows and efforts interchanged. Furthermore, **Transformers (TF)** are physical junctions in which flows and efforts of bonds  $i < j$  connected to them are related such as  $\varphi_{TF}(e_i, e_j) = 0$  and  $\varphi_{TF}(f_j, f_i) = 0$ . Similarly, **Gyrators (GY)** define the following relations  $\varphi_{GY}(e_i, f_j) = 0$  and  $\varphi_{GY}(e_j, f_i) = 0$ .

One of the main advantages of this formalism is domain-agnostic property, as power can be defined in any physical field. For instance, in electricity, effort is voltage, flow is the current; in mechanics,  $e$  is force and  $f$  velocity; in fluid mechanics,  $e$  is pressure and  $f$  velocity.

Another important aspect of the bond graph formalism is the causality, which sets how the equations are written to establish the state system. In particular causality assignment rules [8] guarantee the existence of a solution for the set of equations governing system, the main one being: *exactly one bond imposes the effort (resp. flow) in 0-junction (resp. 1-junction)*.

## 2.2 Preliminaries on Message Passing Graph Neural Networks

MPGNs belong to the class of deep learning algorithms acting on a graph  $G(V, E)$ , where  $V$  are the nodes and  $E$  are the edges. They originate from the adaptation of Convolutional Neural Net-

works (CNNs) on grid graphs to a network acting on a graph with an arbitrary shape [15]. Their main principle consists of updating, within each layer  $l$ , the features  $\mathbf{h}^l(v)$  of each node  $v$  as  $\mathbf{h}^{l+1}(v) = f_{\text{update}}^l(\mathbf{h}^l(v), f_{\text{aggr}}^l(\{\mathbf{h}^l(u) | u \in N(v)\}))$ , where  $u \in N(v)$  are all the nodes such as  $(u, v)$  is an edge.  $f_{\text{update}}$  and  $f_{\text{aggr}}$  define the MPGNs architecture, i.e., how the information is processed across each node,  $\theta_u^l, \theta_a^l$  are parameters updated through the learning process.

## 3 NBgE : a new multi-physical encoder

As the previous section shows, we have bond graphs, which are graphical multi-physical representations operating on continuous physical signals stored in the bonds (edges). On the other hand, we have deep neural models operating on graphs where information is stored in the nodes. In this paper, we develop a method to translate the bond graphs into readable graphs for a deep learning algorithm, where effort and flow variables are stored in nodes instead of edges. Before presenting this translation approach, we detail the assumptions about the physical system and associated bond graph.

### 3.1 Working hypothesis

**Hypothesis 1** (Existence of a connected Bond graph). *We assume that the studied phenomena are governed by physical laws that can be modeled by a connected bond graph.*

**Hypothesis 2** (1D systems and 1D bond graphs). *Only 1D systems and 1D bond graphs are considered. In other words, a bond carries only one effort and flow variable; physical elements (SE, SF, R, I, C) are 1-port elements; physical junctions (TF, GY) are 2-port junctions. The components (elements and junctions) define 1D constitutive relations.*

**Hypothesis 3** (Linear physical relation). *Only proportional element relations, i.e., first-order physical approximations, are considered. Under hypothesis 2, we have for  $\mathcal{BG}(\mathcal{C}, \mathcal{B})$ ,  $\forall \mathcal{C} \in \mathcal{C} | c(\mathcal{C}) \in \{R, I, C, TF, GY\}, \exists \alpha_{\mathcal{C}} \in \mathbb{R}^* | \varphi_{\mathcal{C}}(x, y) = x - \alpha_{\mathcal{C}}y = 0$ .*

### 3.2 A matrix representation of a bond graph

In this section, we define a new representation of a bond graph on which the graph generation process will run.

Given a bond graph  $\mathcal{BG}(\mathcal{C}, \mathcal{B})$ , let denote  $M = \text{card}(\mathcal{B})$  the number of bonds in a bond graph, and  $k(b) \in [1, \dots, M]$  the id of  $b \in \mathcal{B}$ . For clarity, we will write  $b$  instead of  $k(b)$  to identify matrices rows. We introduce the  $M \times 9$  matrix  $\mathcal{BM}$ , representing the bond graph (see Figure 2 where the Bond Matrix of the DC motor is developed). The columns are divided into 2 groups :

- The first group is the *physical element group*. If a bond  $b \in \mathcal{B}$  is connected to a component  $\mathcal{C} \in \mathcal{C}$  of type  $c \in \{\text{SE}, \text{SF}, \text{R}, \text{I}, \text{C}\}$ , then  $\mathcal{BM}[b, c] \neq 0$ . If  $c \in \{\text{SE}, \text{SF}\}$ ,  $\mathcal{BM}[b, c] = k(c)$ . If  $c \in \{\text{R}, \text{I}, \text{C}\}$ ,  $\mathcal{BM}[b, c] = \alpha_c$ ,
- The second group is the *junction-causality group*. We employ triplets here as descriptors as follows : the algebraic id of the junction, the linear physical coefficient and the variable imposed on the junction (i.e. causality). If a bond  $b$  is connected to a junction  $\mathcal{C} \in \mathcal{C}$  of type  $j \in \{\text{TF}, \text{GY}, 0, 1\}$ , then  $\mathcal{BM}[b, j] \neq 0$ . If  $b$  is directed towards  $j$ , then  $\mathcal{BM}[b, j][0] = +k(c(\mathcal{C})) > 0$ , otherwise, it is equal to  $-k(c(\mathcal{C})) < 0$ . If  $j \in \{\text{TF}, \text{GY}\}$ , then  $\mathcal{BM}[b, j][1] = \alpha_c$ , otherwise it is empty. If  $b$ 's causal stroke is at  $j$ 's end, then  $\mathcal{BM}[b, j][2] = e$ , otherwise, it is  $f$ .

With this new representation of a bond graph, thanks to lemma 1 :

**Lemma 1.** *Any bond is connected to a junction.*

We have the following theorem :

**Theorem 1** (Expressiveness of the Bond Matrix). *Any bond graph is fully described by the bond matrix down to the physical elements' ids and effort-flow variables.*

Effort and flow variables correspond to the input data. The ids of the physical components are not informative for us : we care about how they relate  $e$  and  $f$ . This theorem allows us to work with the Bond Matrix for the dual graph generation.

### 3.3 Graph generation process from the Bond Matrix

In this paper we are in the case of a multi-variate time series. Let  $\mathbf{X} \in \mathbb{R}^{N \times D}$  denote a multi-variate time series input with  $N$  timestamps and  $D$  aligned uni-modal channels. Let's assume  $\mathbf{X}$  is generated by a (partially known) multi-physical system represented by a Bond graph  $\mathcal{BG}(\mathcal{C}, \mathcal{B})$ , in other words, an input channel corresponds to an effort or a flow variable of a bond in the bond graph  $\mathcal{BG}(\mathcal{C}, \mathcal{B})$ .

From now, we assume that  $\mathcal{BG}_{\mathbf{X}}(\mathcal{C}, \mathcal{B})$  is complete<sup>1</sup> with respect to  $\mathbf{X}$  and denote  $\mathcal{BM}$  the corresponding Bond Matrix. The goal here is to generate a new graph  $G(V, E)$  representing the data and the multi-physical bond graph knowledge to work on the latent representation of the input channels by performing message passing.

Our methodology is outlined as follows: we first go into the frequency domain with the discrete Fourier transform (DFT). As seen in Section 2.1, physical relation involves temporal integrations, which are temporal convolutions. Going to the frequency domain enables to tackle temporal convolutions as they become frequency multiplications (see integration and derivation matrix operators defined below),

1

**Definition 1** (Completeness). *Let  $\mathbf{X}$  denote a multi-variate input with  $D$  channels. Let  $\mathcal{BG}$  denote a bond graph with  $M$  labeled bonds from 1 to  $M$ . A Bond graph  $\mathcal{BG}(\mathcal{C}, \mathcal{B})$  is complete with respect to  $\mathbf{X}$  if and only if there exists an injective function  $f_{\mathbf{X}, \mathcal{BG}}$  such as :*

$$\forall d \in \{1, \dots, D\}, \exists! b \in \mathcal{B} | f_{\mathbf{X}, \mathcal{BG}}(d) = e_{k(b)} \text{ or } f_{k(b)} \quad (1)$$

which are naturally handled by neural networks [18]. In addition, representations in the frequency domain are sparse and add interpretability [18, 31, 34]. Then, we define a 7-step algorithm taking as input the bond matrix  $\mathcal{BM}$  and  $\hat{\mathbf{X}}$  (DFT of  $\mathbf{X}$ ) and outputs a graph  $G$  which translates the bond graph knowledge in a dual fashion. The first five steps handle 1-port ( $\mathbf{R}, \mathbf{I}, \mathbf{C}$ ), 2-port ( $\mathbf{TF}, \mathbf{GY}$ ), and n-port (0-1 junctions) power processing. The sixth step relaxes causality to add freedom to the dual graph. As all physical signals are not necessarily measured ( $f_{\mathbf{X}, \mathcal{BG}}$  is injective) the final step completes the missing node features of  $G$ . The dual correspondence is described in Table 1. First, let's define the matrix operators in the discrete frequency domain which will constitute the basis of the edge features of the dual graph  $G$ .

Graph	Bond Graph	Bond Graph Convolution
Node	Bond variable (effort or flow)	
Node Label $\mathcal{L}_V$	Bond id and its variable ( $e_{k(b)}$ or $f_{k(b)}$ )	
Node Feature $\mathbf{H}_V$	Sensor data in frequency domain	Message to pass
Edge	Relations between efforts and flows set by the components	
Edge feature $\mathcal{F}_E$	$\varphi_{\mathcal{C}}$ equation in the frequency domain	Unbiased Feed forward network (FFN)
Edge direction	Causality, effort and flow exchange direction	FFN weights

**Table 1.** Correspondence table between the generated AI-readable dual graph, the Bond Graph and the Bond Graph Convolution (Section 3.4)

### Integration and Derivation discrete frequency matrix operators

Let's consider a signal  $x[n]_{n \in 0, \dots, N-1}$  sampled from  $x(t)_{t \in \mathbb{R}} \in \mathbb{R}$  at a frequency  $f_s \in \mathbb{R}_+^*$ . Let denote  $y[\cdot]$  the discrete integral of  $x[\cdot]$ . Using the trapezoidal rule for integration, we have  $y[n] = y[n-1] + \frac{1}{f_s} \frac{x[n-1] + x[n]}{2}, \forall n \in 1, \dots, N-1$ . Taking the Z-transform of this equation and applying it to the Discrete Fourier Transform (DFT) with  $z = e^{\frac{i2\pi k}{N}}, \forall k \in 0, \dots, N-1$ , we have :

$$Y[k] = \frac{1}{2f_s} \frac{e^{\frac{i2\pi k}{N}} + 1}{e^{\frac{i2\pi k}{N}} - 1} X[k], \forall k \in 1, \dots, N-1 \quad (2)$$

We can define the discrete frequency Integration operator  $\mathcal{H}_I$  :  $k \mapsto \frac{1}{2f_s} \frac{e^{\frac{i2\pi k}{N}} + 1}{e^{\frac{i2\pi k}{N}} - 1}, \forall k \in 1, \dots, N-1$ . Conversely, as derivation is the inverse operation of integration, we can define the discrete frequency Derivation operator  $\mathcal{H}_D$  :  $k \mapsto 2f_s \frac{e^{\frac{i2\pi k}{N}} - 1}{e^{\frac{i2\pi k}{N}} + 1}, \forall k \in 0, \dots, N-1$ . In the case of low-frequency modes with  $\frac{k}{N} \ll 1$ , we have the following approximation:  $\mathcal{H}_I[k] \approx \frac{1}{2\pi f_s} \frac{N}{ik}$  and  $\mathcal{H}_D[k] \approx 2\pi f_s \frac{ik}{N}$ , i.e. the same formula as in the continuous case evaluated on the discrete sampled frequencies  $\frac{k}{N} f_s$ .

We extend the linearised formula to any discretised modes as the data is sampled from a continuous phenomenon and as the DFT is a discretisation of the Fourier transform (FT). This formulation considers that points can exist between the sampled ones, and could be recovered as the formula is still valid for any modes in the continuous case. We thus introduce the matrices operators  $\mathcal{I}_N = \text{diag}(0, \mathcal{H}_I[k])_{k \in 1, \dots, N-1}$  and  $\mathcal{D}_N = \text{diag}(\mathcal{H}_D[k])_{k \in 0, \dots, N-1}$  ( $\mathcal{H}_I$  is not defined for  $k = 0$ , we set it at 0 in  $\mathcal{I}_N$ ). so physical relations  $\varphi$  defined in the bond graphs become matrix operations with  $\mathcal{I}_N$  and  $\mathcal{D}_N$ . For instance, with  $f(t) = \alpha_I^{-1} \int_0^t e(\tau) d\tau$ , we get  $\hat{\mathbf{f}}_N = \alpha_I^{-1} \mathcal{I}_N \hat{\mathbf{e}}_N$  for a I-element with  $\hat{\mathbf{f}}_N$  and  $\hat{\mathbf{e}}_N$  the DFT vector of  $f$  and  $e$ . These physical relations in the discrete frequency domain will define the edge features of the dual graph  $G$ .

**Dual graph generation process** We develop the following procedure to build the graph  $G$  from the bond graph represented by  $\mathcal{BM}$ , decomposed in 7 steps (the full process is detailed in Figure 2 in the case of the DC motor) :

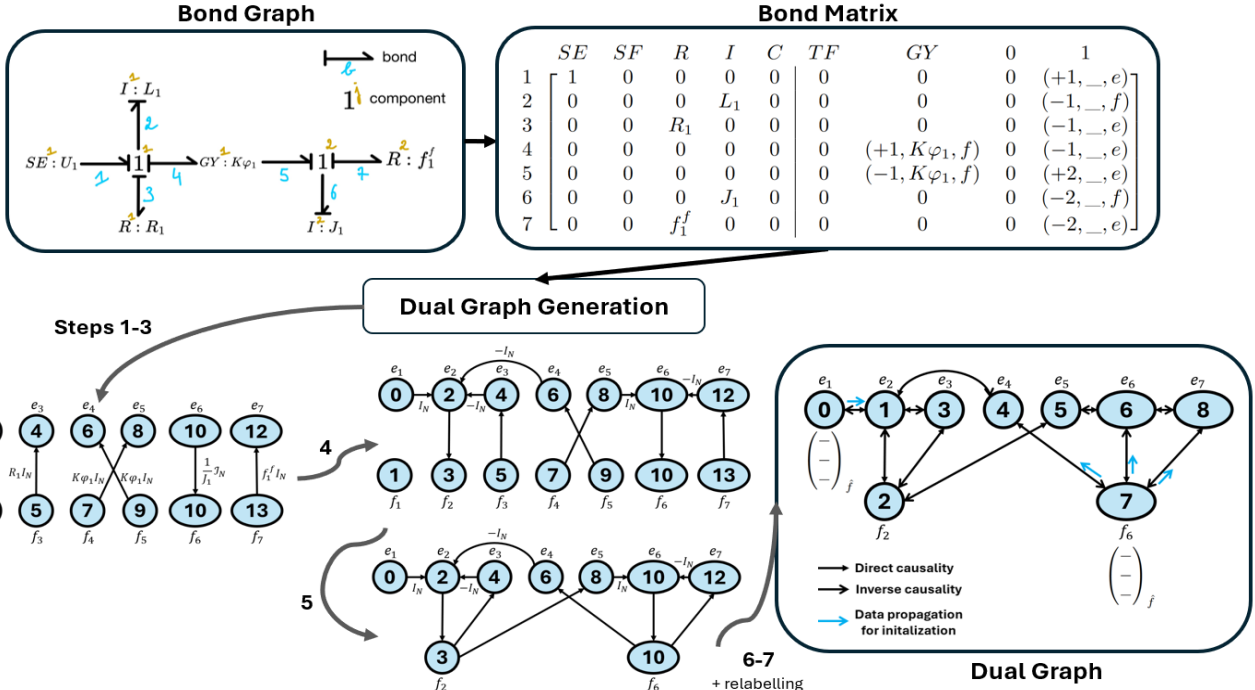


**Figure 2.** From the physical system to the dual graph. The case of the DC Motor is illustrated here. From the bond graph of the system, the Bond Matrix is developed. Then, through the 7-step process, the dual graph is generated. The nodes represent the effort and flow variables, the edges represent the way the power is distributed. Once the dual graph is initialized, the Bond Graph Convolution updates the node features, being the input of the AI forecasting model.

- Initialization:**  $G$  is initialised with  $2 \times M$  nodes, one per variables (effort and flow) per bonds ( $M$  bonds). Each node is labelled by the variable and the bond it represents.  $E = \emptyset$ .
- Physical element relations :** for each bond  $b$  attached to a physical element, i.e. each bond such as  $\exists c \in \{R, I, C\} | \mathcal{BM}[b, c] \neq 0, \exists l \in \{TF, GY, 0, 1\} | \mathcal{BM}[b, l] \neq 0$  (see lemma 1), we add a featured directed edge between  $e_b$  and  $f_b$  depending on the causality in  $\mathcal{BM}[b, l][2]$  and the physical relation. No edge is created for source elements as the effort and flow are independent.
- TF-GY junction relations :** for each bond  $b$ , if  $\mathcal{BM}[b, TF] \neq 0, \exists l \neq b | |\mathcal{BM}[b, TF][0]| = |\mathcal{BM}[l, TF][0]| = k$  (see hypothesis 2) a featured directed edge is added between  $e_b$  and  $e_l$  and between  $f_b$  and  $f_l$  depending on causality and the power direction. Same logic for GY junctions. See [25] for more details on how the equations are written.
- Flow or effort balance at resp. 0 or 1 junctions :** for each 0-junction labelled  $j$ , there exists a unique bond  $b$  such as  $\mathcal{BM}[b, 0][0] = \pm j$  and  $\mathcal{BM}[b, 0][2] = e$  (see causality rules Section 2.1). Then  $b$  receives the flow from the other bonds  $l$  connected to the same junction. We add a featured edge going from the other nodes  $f_l$  to  $f_b$ . Same for 1-junctions replacing flow by effort and vice versa.
- Unique characteristic effort or flow at resp. 0 or 1 junctions :** as in the previous step for the 0-junctions, a unique bond  $b$  imposes the effort at the junction  $j$ . The efforts of the other bonds  $l$  connected to  $j$  are equal to  $e_b$ . We merge the nodes  $e_l$  into  $e_b$ . Same for 1-junctions by replacing efforts by flows.
- Causality reversal :** to give some freedom to the architecture, we revert all edges such that  $\forall (u, v) \in E, (v, u) \in E | \mathcal{F}_E((v, u)) = (\mathcal{F}_E((u, v)))^{-1}$ , with  $\mathcal{I}_N^{-1} = \mathcal{D}_N$ .  $\mathcal{F}_E$  is fully defined. In practice, causality reversal is done together with steps 2, 3, and 4, so edges are created regardless causality. Figure 2 explicitly exhibits causality to understand how the graph ensuring causality should be. We have the following property :

**Property 1** (Connectivity). *The generated graph from the bond graph is connected.*

- Sensor data propagation :** nodes associated with an input channel of  $\mathbf{X}$  are featured with the associated DFT vector. The other nodes don't have any features yet. To give them a feature, information is propagated in a Breadth-first search (BFS) way: we go over each node having sensor information and propagate their message, through the edge features, to their neighbors only once. Previously empty neighbors now have a message to transmit. The latter transmit their messages, etc... As the graph is connected, we end the procedure when all the nodes have been visited exactly once. We average all the messages received by each node during the procedure. We go back to the temporal domain to get the final initialization. Only previously empty nodes are updated during this procedure.  $\mathbf{H}_V$  is fully defined.

The whole procedure is detailed in Section ??.

The directed node-labeled and node-edge-attributed graph  $G(V, E, \mathcal{L}_V, \mathbf{H}_V, \mathcal{F}_E)$  is completely defined, and we can perform message passing over it thanks to the Bond Graph Convolution, a physical-informed MPGNN.

### 3.4 The Bond Graph Convolution

We introduce a new MPGNN called the Bond Graph Convolution (BGC). Instead of tuning a global message passing over a graph as in [10, 15, 30], we learn a specific message passing over each physical-informed edge. Using the same notations as in section 2.2,  $f_{\text{update}}$  is the mean function, and  $f_{\text{aggr}}$  is the same as in [15] but, instead of a global matrix that processes the message passing,  $f_{\text{aggr}}$  depends on the edges such as the matrices processing the messages are the edge features  $\{\Phi_{(u,v)}^l\}_{(u,v) \in E}$  updated through the learning process.

We chose to model the linear bond graph relations in the discrete frequency domain as an unbiased 1-layer Feed forward network

(FFN)  $\Phi$  initialized with the known physical relations. In the previous example, if  $b \in \mathcal{B}$  is connected to a I-element, we would have  $\Phi_{(e_b, f_b)}^{l, \text{init}} = \alpha_I^{-1} \mathcal{I}_{d_l}$ , where  $e_b$  and  $f_b$  are the nodes of bond  $b$ 's effort and flow and  $d_l$  the dimension of layer  $l$ .

---

**Algorithm 1** The Bond Graph Convolution at a layer  $l$ 


---

```

Input  $G, \mathbf{H}_V^{l-1}$ 
Output  $\mathbf{H}_V^l$ 
1:  $\mathbf{H}_V^l \leftarrow \mathbf{0}_{|V| \times d_l}$ 
2: for  $i$  in  $V$  do
3:    $\mathbf{H}_{V,i}^l \leftarrow \frac{1}{\text{card}(\mathcal{N}_i \cup \{i\})} (\sum_{j \in \mathcal{N}_i} \mathbf{H}_{V,j}^{l-1} \Phi_{(j,i)}^l + \mathbf{H}_{V,i}^{l-1})$ 
4: end for

```

---

During the learning process,  $\{\Phi_{(u,v)}^l\}_{(u,v) \in E}$  are updated: non-linear physical phenomena can be learned as non-diagonal weights appear.

### 3.5 Building the Neural Bond Graph Encoder

From the BGC, we build a Bond Graph Layer (BGL) :

$$\hat{\mathbf{H}}_s^{l-1} = \text{Sampling}(DFT(\mathbf{H}^{l-1})) \quad (3)$$

$$\hat{\mathbf{H}}_s^{l-1} = BGC^l(\hat{\mathbf{H}}_s^{l-1}) \quad (4)$$

$$\tilde{\mathbf{H}}^{l-1} = \text{Padding}(DFT^{-1}(\hat{\mathbf{H}}_s^{l-1}), \mathbf{H}^{l-1}) \quad (5)$$

$$\mathbf{H}^l = \sigma((0.8 \cdot \tilde{\mathbf{H}}^{l-1} + 0.2 \cdot \mathbf{H}^{l-1})W^l + B^l) \quad (6)$$

with  $DFT$  the Discrete Fourier Transform,  $\sigma$  an activation function,  $W^l \in \mathbf{R}^{d_l \times d_l}$  and  $B^l \in \mathbf{R}^{d_l}$ , with  $d_l$  the dimension of the layer. We perform Sampling (defined in [34]) and Padding operations to make the most of the sparse property of the TF. The equations developed in the previous sections remain the same, replacing the vectors and matrices by their extraction on the sampled modes. The Padding consists of updating the selected modes from the Sampling on the input features  $\mathbf{H}^{l-1}$ . The weighting coefficients in equation 6 were found empirically.

Then, we stack a scalar layer [18] (layer 0) and  $L$  BGL in series, and we perform Cross Attention [13] to compute the output of what we call the Neural Bond Graph Encoder (NBgE) :

$$\mathbf{H}^{out} = \sum_{l=1}^L (\mathbf{H}^l \Phi_a^l + B_a^l) \quad (7)$$

## 4 Experimental study

### 4.1 Datasets

We test NBgE on two challenging physical systems in two opposite quality of physical knowledge with the same amount of data and equivalent samples. On the one hand, we have our own simulated dataset of a Direct Current motor. We fully know the system, so the associated bond graph perfectly represents the system behavior. On the other hand, we have the respiratory system taken from the experiments conducted by [9]. No explicit equations with the variables of interest exist and no bond graph has been developed for this specific case. We barely have a physical knowledge of the system and the data is noisy. It is a very challenging setup for our methodology. More details on both datasets are available in the supplementary material.

### 4.1.1 The DC motor

The DC motor has two domains: the electrical and mechanical ones. In the electrical part, a voltage source  $U_1$  powers up a resistance  $R_1 = 5 \Omega$  and an inductance  $L_1 = 0.1\text{H}$  in series and an electro-mechanical  $K\varphi_1 = 0.1 \text{ V.s.rad}^{-1}$  converter attached to a shaft  $J_1 = 0.01 \text{ kg.m}^2$  subjected to fluid fiction  $f_1^f = 0.001 \text{ N.m.s.rad}^{-1}$  (the bond graph and bond matrix are developed in Figure 1 and 2). The DC motor model and simulation are performed on MATLAB SIMULINK. To generate the signals, we set the voltage source as a square signal going from 0 to 2 V with a variable frequency and pulse sweep. We add to it some controlled noise: every 10 seconds,  $U_1$  is multiplied by a constant uniformly sampled between 0.8 and 1.2. The accessible channels are the voltage current and the shaft rotation speed. The problem is ill-posed as the DC motor equations require the voltage source to be solved numerically.

### 4.1.2 The respiratory system

The respiratory system has two domains: the fluid and the mechanical ones. The former corresponds to the air and the latter to the trachea distension, the lungs movement, the muscles action, the chest and abdomen movement. The latter combines elements of multiple physical nature. The data has been recorded by [9] across 80 people in order to develop automatic methods to monitor patients with respiratory diseases. To employ our methodology, a complete bond graph is needed. Our starting point is the bond graph of the lungs developed in [1] where the trachea and the lungs are modeled. The chest-abdomen part is missing. To add it, we conducted a power transmission reasoning: the lungs swelling - modeled as a balloon - induces the displacement of the chest and the abdomen thanks to the diaphragm. In our case, the accessible channels are the air pressure and flow in the trachea, the displacement of the chest and the abdomen. We normalize the data of each channel between 0 and 1 to set the bond graph parameters values to 1 as they are unknown.

### 4.2 Experimental Setup

We choose the challenging forecasting task to assess the performances of the NBgE methodology. Let  $\mathbf{X} = \{X_1^t, \dots, X_D^t\}_{t=1}^N$  denote the historical data of  $N$  timestamps. The time series forecasting task is to infer  $K$  future timestamps based on the  $N$  historical ones  $\hat{\mathbf{X}} = \{\hat{X}_1^t, \dots, \hat{X}_D^t\}_{t=N+1}^{N+K}$ . On both datasets, to build up the samples for the task, we set a window of 600 points per channel, and we extract them (without overlaps) from randomly chosen recordings to get a total of around 500 samples for the task. We test the models on three scenarios :  $(N = 100, K = 500)$ ,  $(N = 300, K = 300)$ , and  $(N = 500, K = 100)$ . To assess the model agnostic property of the NBgE, we choose 4 models being the basis of the majority of AI models: Linear [32], Multi-Perceptron Layers (MLP), GraphSAGE [10] and Transformer [29]. We omit PINNs in our comparison as the listed models take the  $N$  points per channel as input, whereas PINNs take the timestamp as input, and our purpose is to compare NBgE-informed models against non-informed ones. We take one configuration performing quite well for each model on each physical system and compare their performance with and without the NBgE. For each case, the hyperparameters of the encoder, the epochs, the learning rate and the linear decreasing rate<sup>2</sup> are tuned with the help of Tune and HyperOpt [3, 19].

---

<sup>2</sup> during the learning process, the learning rate decreases linearly from the initial value  $lr$  to  $(\text{decreasing rate}) \times lr$

Study case		Linear		MLP		GraphSAGE		Transformer	
DC motor		w/o	w/	w/o	w/	w/o	w/	w/o	w/
100-500	MAE	3.912 $\pm$ 0.002	<b>1.639 <math>\pm</math> 0.031</b>	1.526 $\pm$ 0.036	<b>1.367 <math>\pm</math> 0.029</b>	1.478 $\pm$ 0.013	<b>1.317 <math>\pm</math> 0.024</b>	<b>1.312 <math>\pm</math> 0.038</b>	1.345 $\pm$ 0.047
	MSE	52.72 $\pm$ 0.06	<b>13.07 <math>\pm</math> 0.39</b>	14.70 $\pm$ 0.45	<b>11.32 <math>\pm</math> 0.36</b>	15.98 $\pm$ 0.47	<b>10.17 <math>\pm</math> 0.48</b>	<b>9.701 <math>\pm</math> 0.491</b>	10.18 $\pm$ 0.93
	SDTW	20335 $\pm$ 68	<b>4553 <math>\pm</math> 155</b>	5977 $\pm$ 279	<b>3685 <math>\pm</math> 207</b>	6262 $\pm$ 239	<b>3559 <math>\pm</math> 146</b>	<b>2792 <math>\pm</math> 256</b>	2954 $\pm$ 525
	# param. (M)	0.051	1.1	2.2	4.1	4.8	6.1	26.3	28.6
300-300	MAE	3.055 $\pm$ 0.005	<b>1.264 <math>\pm</math> 0.018</b>	<b>1.262 <math>\pm</math> 0.024</b>	1.270 $\pm$ 0.032	<b>1.167 <math>\pm</math> 0.020</b>	1.226 $\pm$ 0.036	<b>0.964 <math>\pm</math> 0.073</b>	0.981 $\pm$ 0.023
	MSE	33.16 $\pm$ 0.05	<b>9.347 <math>\pm</math> 0.636</b>	<b>7.443 <math>\pm</math> 0.262</b>	7.662 $\pm$ 0.303	<b>6.987 <math>\pm</math> 0.175</b>	7.300 $\pm$ 0.222	5.874 $\pm$ 0.648	<b>5.583 <math>\pm</math> 0.436</b>
	SDTW	6728 $\pm$ 68	<b>2370 <math>\pm</math> 176</b>	<b>2040 <math>\pm</math> 113</b>	2065 $\pm$ 94	<b>1802 <math>\pm</math> 37</b>	1889 $\pm$ 71	<b>1027 <math>\pm</math> 142</b>	1048 $\pm$ 85
	# param. (M)	0.09	2.0	2.3	4.2	4.8	7.5	26.3	28.2
500-100	MAE	1.810 $\pm$ 0.010	<b>0.893 <math>\pm</math> 0.024</b>	<b>0.597 <math>\pm</math> 0.028</b>	0.663 $\pm$ 0.027	<b>0.524 <math>\pm</math> 0.007</b>	0.637 $\pm$ 0.026	<b>0.705 <math>\pm</math> 0.060</b>	0.711 $\pm$ 0.041
	MSE	11.73 $\pm$ 0.09	<b>5.529 <math>\pm</math> 0.374</b>	<b>2.863 <math>\pm</math> 0.297</b>	3.900 $\pm$ 0.433	<b>2.583 <math>\pm</math> 0.080</b>	3.697 $\pm$ 0.344	3.750 $\pm$ 0.499	<b>3.511 <math>\pm</math> 0.408</b>
	SDTW	1464 $\pm$ 15	<b>630.8 <math>\pm</math> 52.2</b>	<b>322.6 <math>\pm</math> 53.6</b>	418.0 $\pm$ 64.8	<b>316.5 <math>\pm</math> 12.4</b>	395.4 $\pm$ 36.4	243.6 $\pm$ 32.7	<b>227.0 <math>\pm</math> 29.8</b>
	# param. (M)	0.051	3.0	2.4	5.0	4.8	7.6	26.3	27.8
Respiratory system		w/o	w/	w/o	w/	w/o	w/	w/o	w/
100-500	MAE	12.53 $\pm$ 0.01	<b>11.70 <math>\pm</math> 0.03</b>	13.12 $\pm$ 0.14	<b>11.59 <math>\pm</math> 0.02</b>	12.18 $\pm$ 0.10	<b>11.77 <math>\pm</math> 0.10</b>	<b>11.74 <math>\pm</math> 0.04</b>	11.75 $\pm$ 0.02
	MSE	3.274 $\pm$ 0.002	<b>2.983 <math>\pm</math> 0.031</b>	3.357 $\pm$ 0.047	<b>2.859 <math>\pm</math> 0.023</b>	3.127 $\pm$ 0.063	<b>2.917 <math>\pm</math> 0.045</b>	2.999 $\pm$ 0.063	<b>2.947 <math>\pm</math> 0.024</b>
	SDTW	64.33 $\pm$ 0.06	<b>54.04 <math>\pm</math> 1.30</b>	62.12 $\pm$ 2.28	<b>58.97 <math>\pm</math> 0.63</b>	61.43 $\pm$ 1.75	<b>56.20 <math>\pm</math> 1.73</b>	<b>55.01 <math>\pm</math> 3.85</b>	58.82 $\pm$ 1.08
	# param. (M)	0.051	10.7	1.4	11.9	4.2	18.6	8.4	28.1
300-300	MAE	11.70 $\pm$ 0.009	<b>9.740 <math>\pm</math> 0.047</b>	10.96 $\pm$ 0.175	<b>9.826 <math>\pm</math> 0.120</b>	10.30 $\pm$ 0.058	<b>10.19 <math>\pm</math> 0.12</b>	10.97 $\pm$ 0.13	<b>10.61 <math>\pm</math> 0.16</b>
	MSE	2.948 $\pm$ 0.006	<b>2.315 <math>\pm</math> 0.032</b>	2.522 $\pm$ 0.068	<b>2.368 <math>\pm</math> 0.063</b>	2.321 $\pm$ 0.046	2.375 $\pm$ 0.056	2.924 $\pm$ 0.132	<b>2.618 <math>\pm</math> 0.088</b>
	SDTW	28.26 $\pm$ 0.09	<b>21.78 <math>\pm</math> 0.23</b>	26.35 $\pm$ 0.61	<b>20.85 <math>\pm</math> 0.70</b>	24.29 $\pm$ 0.77	<b>22.03 <math>\pm</math> 0.78</b>	24.20 $\pm$ 0.309	<b>23.12 <math>\pm</math> 1.61</b>
	# param. (M)	0.09	9.7	1.4	11.0	4.2	18.1	8.4	70.8
500-100	MAE	10.33 $\pm$ 0.01	<b>8.844 <math>\pm</math> 0.157</b>	<b>8.701 <math>\pm</math> 0.181</b>	8.715 $\pm$ 0.135	<b>8.747 <math>\pm</math> 0.166</b>	8.753 $\pm$ 0.119	8.580 $\pm$ 0.293	<b>8.366 <math>\pm</math> 0.126</b>
	MSE	2.465 $\pm$ 0.007	<b>1.764 <math>\pm</math> 0.056</b>	<b>1.670 <math>\pm</math> 0.054</b>	1.722 $\pm$ 0.057	<b>1.696 <math>\pm</math> 0.064</b>	1.707 $\pm$ 0.040	1.789 $\pm$ 0.117	<b>1.725 <math>\pm</math> 0.088</b>
	SDTW	8.775 $\pm$ 0.093	<b>6.771 <math>\pm</math> 0.154</b>	<b>6.527 <math>\pm</math> 0.402</b>	6.577 $\pm$ 0.273	<b>5.954 <math>\pm</math> 0.231</b>	6.565 $\pm$ 0.229	<b>5.495 <math>\pm</math> 0.670</b>	5.542 $\pm$ 0.258
	# param. (M)	0.051	26.8	1.4	28.2	4.2	14.8	8.4	18.0

**Table 2.** Non-informed models (w/o) performances compared to the multi-physical-informed ones with NBgE (w/). For each metric, the lower, the better. The best scores between the informed and non-informed models are in **bold**, and the overall best scores are underlined. (Respiratory system’s MAE and MSE score are  $\times 10^{-2}$ )

In each case, we take 80% of the samples for training (with 10% for validation) and 20% for testing. We choose the Huber Loss ( $\delta = 0.1$ ) to train all the models based on [12]. Our metrics comparison are the Mean Average Error (MAE), the Mean Square Error (MSE), and the Soft Dynamic Time Warping (SDTW) ( $\gamma = 0.1$ ) [5]. The first two are basic metrics for time series forecasting tasks; the latter controls the shape similarity between targets and predictions.

### 4.3 Overall Comparisons

We can observe, from the results in Table 2, that in the following cases: DC Motor ( $N = 100; K = 500$ ), Respiratory system ( $N = 100; K = 500$ ) and ( $N = 300; K = 300$ ), informed models get better results than the non-informed ones in general. This could correspond to the *some physics, some data* [14] setup. Despite the limited knowledge of the respiratory system, NBgE generates more informative representations of the data. The encoder in the DC motor case, where the knowledge is more precise, is smaller than the encoder in the respiratory system case. In the respiratory study case, NBgE-informed MLP and Linear get better results than the non-informed Transformer, which would support the encoder’s benefits, being more expressive than the transformer here. Predictions on both datasets are displayed in Figure 3 to show the improvements thanks to NBgE.

### 4.4 Ablation study

To assess the architecture choices, we compare our model to the following ones: **w/o CA**: NBgE without the Cross Attention aggregation, **w/o Phy feat**: nodes without any associated input channel are initialized with random features, **w/o Phy Init & w/o phy feat**: it is w/o Phy feat, and, in addition, the FFN edge features are randomly initialized. The results are shown in Table 3. Overall, our model gets the best results across the two study cases. However, the **w/o Phy Init & w/o phy feat** model gets similar results to ours: the inductive bias of the encoder’s architecture seems more informative than the physical-informed initialization of the node and edge features.

Study case		ours	w/o CA	w/o Phy Feat	w/o Phy Init & phy feat
DC Motor 100-500	MAE	1.367 $\pm$ 0.029	<b>1.366 <math>\pm</math> 0.023</b>	1.413 $\pm$ 0.025	1.393 $\pm$ 0.026
	MSE	11.32 $\pm$ 0.36	12.13 $\pm$ 0.55	12.07 $\pm$ 0.34	<b>10.87 <math>\pm</math> 0.25</b>
	SDTW	<b>3685 <math>\pm</math> 207</b>	4223 $\pm$ 267	4094 $\pm$ 258	3706 $\pm$ 133
Resp. sys 100-500	MAE ( $\times 10^{-2}$ )	<b>11.59 <math>\pm</math> 0.02</b>	11.89 $\pm$ 0.05	11.71 $\pm$ 0.02	11.73 $\pm$ 0.02
	MSE ( $\times 10^{-2}$ )	<b>2.859 <math>\pm</math> 0.023</b>	2.991 $\pm$ 0.013	2.990 $\pm$ 0.015	2.905 $\pm$ 0.017
	SDTW	<b>58.97 <math>\pm</math> 0.063</b>	69.41 $\pm$ 1.56	60.76 $\pm$ 0.30	60.96 $\pm$ 0.41

**Table 3.** Ablation study on the two physical systems with the forecasting task ( $N = 100, K = 500$ ) on the MLP model informed by NBgE without some constraints. Results are quite similar between the models for the respiratory system: the inductive bias of the architecture is predominant.

### 5 Related work

**Physical-Informed Neural Network** PINNs architectures [23] take as input the space-time location and output the state of the studied system at the input location. The residuals of the equations governing the data are added to the loss of the network during training: the more physical domain, the more equations, the more hyperparameters to tune. There isn’t any unified framework for multiphysics [14] yet. For instance, in [4], heat transfer is studied between the air and a wall. To address the multi-physical domain, they define two separate PINNs - one for the fluid and one for the solid domain - coupled by a global loss trained for the solid and fluid domain.

**Physical-Informed Graph Neural Networks** Graph Neural Networks (GNNs) are widely used for physical applications as they are equivariant to permutation by design. However, one would like the model to have additional equivariances transcribing the system’s physical properties. In [16, 33, 17, 27], they design a specific message passing algorithm on the molecular graph, invariant and equivariant to targeted transformations. In [21], they define a new class of GNNs to relax the equivariance to permutation to get different predictions on similar nodes, such as atoms.

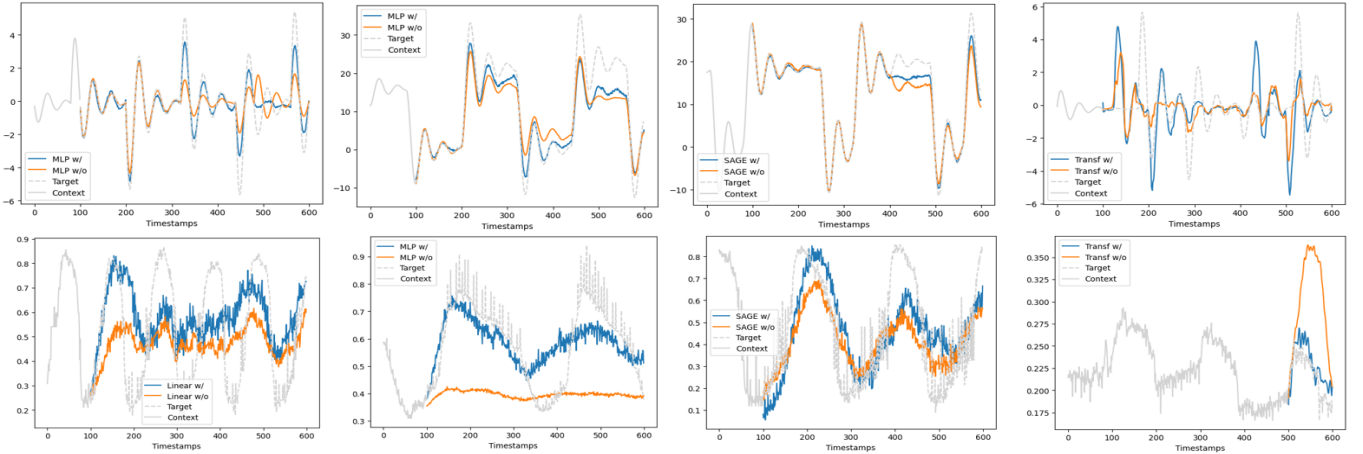


**Figure 3.** At the top line, predictions on the channels of the DC motor datasets, at the bottom line, predictions on the Respiratory dataset. In blue, the NBgE informed model against the non-informed one in orange.

**Bond graphs and ML** Several papers have worked on combining Bond graphs and ML models. The bond graph formalism models each part of the studied system. It is pretty interesting in a Fault Detection and Isolation (FDI) framework. Indeed, thanks to the Bond graph, we can identify and isolate the causes of the system’s faulty behavior, which is quite helpful for maintenance purposes. In [6], they combine the residuals generated by the bond graph [26] and a Convolution Neural Network (CNN) to classify the fault and compute the contribution of each part of the system to it. Graphs are a standard structure to work on the data; bond graphs can help generate one and run a model on it. In [20], they generate a Bayesian network from the bond graph and compute the probability of being dysfunctional over each component of the bond graph. In the case of complex systems, Bond graphs can suffer from numerical issues such as algebraic loops [8]. AI models can help bond graphs simplify the equations and solve the system’s governing equations. [11] identifies the principle variables that govern the system thanks to a Principal Component Analysis (PCA). Then, from the former variables, neural networks recover the other variables, simplifying the overall system equations. The associations between Bond graphs to help AI models are quite restricted to the FDI task. No attempts have been made to develop a method of mixing Bond graph and AI formalism in a general informed framework for other tasks such as classification and forecasting.

## 6 Conclusion

We propose the first contribution that leverages the bond graph formalism through graph neural networks. We propose NBgE, an unified framework that can inform any AI model and tackle any bond graphs multi-physics systems (under the working hypothesis). We show the benefits of our approach on the time series forecasting task on two datasets: a simulated one (DC motor) and a real-measured one (Respiratory system [9]). We conduct exhaustive experiments on four AI prediction models, going from the simplest one (Linear [32]) to the Transformer [29] and an ablation study to assess the impact of our choices on NBgE.

A clear trend confirms the benefits of adding physical knowledge in the *some physics, some data* [14] setup. Even when the system’s knowledge is approximative, NBgE can produce better data representations. Choices made on the BGC and learning process are basic, so refinements can be done on NBgE to generalize the observed trend. A deeper study should be done on the inverse trend of the in-

formed Transformer compared to the other models. This work is a first attempt and there are opportunities to get more potent results. In addition, physical laws identification on the updated edge features could be considered. Potential applications are possible, such as training NBgE in an unsupervised way as BERT [7] and employing in a downstream task, or integrating NBgE in the pipeline of [28] thanks to a 3D bond graph modelization of fluid dynamics [2]. All of these points are considered as future work for us.

## References

- [1] A. Arshad, A. Kashif, M. Wasim, N. Mazhar, and T. Zaidi. Bond graph modeling of lungs. pages 1–4, 11 2018. doi: 10.1109/ICECUBE.2018.8610994.
- [2] J. Balleño, A. Larreteguy, and E. G. Raso. A general bond graph approach for computational fluid dynamics. *Simulation Modelling Practice and Theory*, 14(7):884–908, 2006. ISSN 1569-190X. doi: <https://doi.org/10.1016/j.simpat.2006.03.001>. URL <https://www.sciencedirect.com/science/article/pii/S1569190X0600027X>.
- [3] J. Bergstra, D. Yamins, D. D. Cox, et al. Hyperopt: A python library for optimizing the hyperparameters of machine learning algorithms. 2013.
- [4] G. Coulaud and R. Duvigneau. Physics-Informed Neural Networks for Multiphysics Coupling: Application to Conjugate Heat Transfer. Technical Report RR-9520, Université Côte d’Azur, Inria, CNRS, LJAD, Oct. 2023. URL <https://inria.hal.science/hal-04225990>.
- [5] M. Cuturi and M. Blondel. Soft-dtw: a differentiable loss function for time-series, 2018.
- [6] B. M. Dash, B. O. Bouamama, M. Boukerdj, and K. M. Pekpe. Bond graph-cnn based hybrid fault diagnosis with minimum labeled data. *Engineering Applications of Artificial Intelligence*, 131:107734, 2024. ISSN 0952-1976. doi: <https://doi.org/10.1016/j.engappai.2023.107734>. URL <https://www.sciencedirect.com/science/article/pii/S0952197623019188>.
- [7] J. Devlin, M.-W. Chang, K. Lee, and K. Toutanova. Bert: Pre-training of deep bidirectional transformers for language understanding, 2019.
- [8] D.-T. Genivière. *Les bond graphs*. IC2 Information, commande, communication Systèmes automatisés. Paris: Hermès science , DL 2000, 2000. ISBN 2-7462-0158-5.
- [9] E. F. S. Guy, J. A. Clifton, T. Caljé-van Der Klei, R. Chen, J. Knopp, K. Moeller, and J. G. Chase. Respiratory dataset from peep study with expiratory occlusion v1.0.0, Nov. 2023. URL <https://physionet.org/content/respiratory-dataset/1.0.0/>.
- [10] W. L. Hamilton, R. Ying, and J. Leskovec. Inductive representation learning on large graphs, 2018.
- [11] Y. Hammadi, D. Ryckelynck, and A. El-Bakkali. Data-driven reduced bond graph for nonlinear multiphysics dynamic systems. *Applied mathematics and computation*, 409:126359, 2021. ISSN 0096-3003.
- [12] A. Jadon, A. Patil, and S. Jadon. A comprehensive survey of regression based loss functions for time series forecasting, 2022.
- [13] M. Jin, Y. Zheng, Y.-F. Li, S. Chen, B. Yang, and S. Pan. Multivariate time series forecasting with dynamic graph neural odes. *IEEE Transactions on Knowledge and Data Engineering*, 35(9):9168–9180,

Sept. 2023. ISSN 2326-3865. doi: 10.1109/TKDE.2022.3221989. URL <http://dx.doi.org/10.1109/TKDE.2022.3221989>.

- [14] G. E. Karniadakis, I. G. Kevrekidis, L. Lu, P. Perdikaris, S. Wang, and Y. Liu. Physics-informed machine learning. *Nature Reviews Physics*, 3(6):422–440, 2021. doi: 10.1038/s42254-021-00314-5. URL <https://doi.org/10.1038/s42254-021-00314-5>.
- [15] T. N. Kipf and M. Welling. Semi-supervised classification with graph convolutional networks, 2017.
- [16] A. Klipfel, O. Peltre, N. Harrati, Y. Fregier, A. Sayede, and Z. Bouraoui. Equivariant message passing neural network for crystal material discovery, 2023.
- [17] B. Li, Y. Liu, H. Sun, R. Zhang, Y. Xie, K. Foo, F. S. Mak, R. Zhang, T. Yu, S. Lin, P. Wang, and X. Wang. Regio-mpnn : Predicting regioselectivity for general metal-catalyzed cross-coupling reactions using chemical knowledge informed message passing neural network. *ChemRxiv*, 2024. doi: 10.26434/chemrxiv-2024-tddfc. URL <https://doi.org/10.26434/chemrxiv-2024-tddfc>.
- [18] Z. Li, N. B. Kovachki, K. Azizzadenesheli, B. Liu, K. Bhattacharya, A. M. Stuart, and A. Anandkumar. Fourier neural operator for parametric partial differential equations. *CoRR*, abs/2010.08895, 2020. URL <https://arxiv.org/abs/2010.08895>.
- [19] R. Liaw, E. Liang, R. Nishihara, P. Moritz, J. E. Gonzalez, and I. Stoica. Tune: A research platform for distributed model selection and training. *arXiv preprint arXiv:1807.05718*, 2018.
- [20] C. Lo, Y. Wong, and A. Rad. Bond graph based bayesian network for fault diagnosis. *Applied Soft Computing*, 11(1):1208–1212, 2011. ISSN 1568-4946. doi: <https://doi.org/10.1016/j.asoc.2010.02.019>. URL <https://www.sciencedirect.com/science/article/pii/S1568494610000645>.
- [21] M. Morris, B. C. Grau, and I. Horrocks. Orbit-equivariant graph neural networks. In *The Twelfth International Conference on Learning Representations*, 2024. URL <https://openreview.net/forum?id=GkJOCga62u>.
- [22] H. Paynter. Generalizing the concepts of power transport and energy ports for system engineering. In *ASME Presented at the 1958 Annual Meeting New York, NY*, 1958.
- [23] M. Raissi, P. Perdikaris, and G. Karniadakis. Physics-informed neural networks: A deep learning framework for solving forward and inverse problems involving nonlinear partial differential equations. *Journal of Computational Physics*, 378:686–707, 2019. ISSN 0021-9991. doi: <https://doi.org/10.1016/j.jcp.2018.10.045>. URL <https://www.sciencedirect.com/science/article/pii/S0021999118307125>.
- [24] V. L. Rolle, A. Hernández, P.-Y. Richard, J. Buisson, and G. Carrault. A bond graph model of the cardiovascular system. *Acta Biotheoretica*, 53(4):295–312, 2005. doi: 10.1007/s10441-005-4881-4. URL <https://doi.org/10.1007/s10441-005-4881-4>.
- [25] R. Rosenberg and A. Andry. Solvability of bond graph junction structures with loops. *IEEE Transactions on Circuits and Systems*, 26(2):130–137, 1979. doi: 10.1109/TCS.1979.1084615.
- [26] A. Samantaray, K. Medjaher, B. Ould Bouamama, M. Staroswiecki, and G. Dauphin-Tanguy. Diagnostic bond graphs for online fault detection and isolation. *Simulation Modelling Practice and Theory*, 14(3):237–262, 2006. ISSN 1569-190X. doi: <https://doi.org/10.1016/j.simpat.2005.05.003>. URL <https://www.sciencedirect.com/science/article/pii/S1569190X05000717>.
- [27] V. G. Satorras, E. Hoogeboom, and M. Welling. E(n) equivariant graph neural networks, 2022.
- [28] J. Steeven, N. Madiha, D. Julie, and W. Christian. Space and time continuous physics simulation from partial observations, 2024.
- [29] A. Vaswani, N. Shazeer, N. Parmar, J. Uszkoreit, L. Jones, A. N. Gomez, L. Kaiser, and I. Polosukhin. Attention is all you need. *CoRR*, abs/1706.03762, 2017. URL <http://arxiv.org/abs/1706.03762>.
- [30] P. Veličković, G. Cucurull, A. Casanova, A. Romero, P. Liò, and Y. Bengio. Graph attention networks, 2018.
- [31] K. Yi, Q. Zhang, L. Cao, S. Wang, G. Long, L. Hu, H. He, Z. Niu, W. Fan, and H. Xiong. A survey on deep learning based time series analysis with frequency transformation, 2023.
- [32] A. Zeng, M. Chen, L. Zhang, and Q. Xu. Are transformers effective for time series forecasting?, 2022.
- [33] Z. Zhang, M. Xu, A. Jamasb, V. Chenthamarakshan, A. Lozano, P. Das, and J. Tang. Protein representation learning by geometric structure pre-training, 2023.
- [34] T. Zhou, Z. Ma, Q. Wen, X. Wang, L. Sun, and R. Jin. Fedformer: Frequency enhanced decomposed transformer for long-term series forecasting. *CoRR*, abs/2201.12740, 2022. URL <https://arxiv.org/abs/2201.12740>.